

Ti distribution in grain-size fractions of Apollo soils 10084 and 71501



W.G. Kong^{a,b,*}, B.L. Jolliff^b, Alian Wang^b

^a MLR Key Laboratory of Saline Lake Resources and Environments, Institute of Mineral Resources, CAGS, Beijing 100037, China

^b Department of Earth and Planetary Sciences and the McDonnell Center for the Space Sciences, Washington University in St. Louis, St. Louis, MO 63130, USA

ARTICLE INFO

Article history:

Received 20 December 2012

Revised 4 July 2013

Accepted 6 July 2013

Available online 16 July 2013

Keywords:

Moon, Surface

Regoliths

Spectroscopy

ABSTRACT

Much work has been devoted to the correlation between the remotely sensed UV–VIS slope and the TiO₂ concentration of the lunar surface, and this correlation has been used to map the lunar surface TiO₂ distributions using data obtained from various missions. However, additional work is needed to fully evaluate the UV–VIS–TiO₂ correlation. Such work would help ongoing efforts to improve TiO₂ mapping (e.g., as currently underway with LROC Wide Angle Camera (WAC) data). To evaluate the UV–VIS–TiO₂ correlation, we are investigating soil petrographic factors (e.g., modal abundances of Ti bearing minerals, lithic, and glass hosts, ilmenite morphology, grain size, and maturity) that may influence the spectra. This “ground truth” approach will be useful in comparing between sample information and laboratory spectra to investigate the influence of petrographic factors on the spectra. In this work, we report the quantitative results of a systematic laboratory investigation of three size fractions (210–100 μm, 100–48 μm, 48–20 μm) of two high Ti lunar soils 10084 and 71501 using a combined digital imaging (backscattered electron image and X-ray maps) method. For each size fraction, the results include: (1) the modal abundances for single phase minerals and lithologic components; (2) the Ti distributions among Ti host components; and (3) the shape of ilmenite grains. We compile and compare the data together for the three size fractions of the two high Ti soils with different maturities as well as data from previous studies. Future work will include the investigation of finer size fractions (<20 μm) and more samples (Apollo 12, Apollo 15) covering a larger range of Ti concentration and maturity, and comparison with their spectra.

© 2013 Elsevier Inc. All rights reserved.

1. Introduction

Remote sensing plays an important role in determining the distribution of lunar minerals, and the ultraviolet–visible (UV–VIS) ratio of surface reflectance is a widely used parameter to estimate the TiO₂ abundance of mare regolith developed on mare basalt surfaces (e.g., Charette et al., 1974; Johnson et al., 1977, 1991a, 1991b; Pieters et al., 1976; Pieters, 1978; Melendrez et al., 1994; Lucey et al., 1998; Jolliff et al., 1999; Gillis et al., 2003, 2006; Shkuratov et al., 2011). In these works, relations between the UV–VIS band ratio and the TiO₂ content were derived, which were further used to develop band ratio maps for mapping the TiO₂ abundance of the lunar surface. Although the selection of UV–VIS bands strongly depends on specific mission or source of spectra, these TiO₂ mapping efforts are generally carried out on the basis of the Charette relation. Charette et al. (1974) found that lunar surface materials with high-Ti concentration had a lower UV–VIS slope than those with low-Ti concentration through the analysis of remotely sensed spectra obtained on sampled sites, and they used this rela-

tion to map the TiO₂ abundance of the lunar surface. The UV–VIS ratio has a first-order dependence on the ilmenite (FeTiO₃) volume percentage, thus the Charette relation works well for high-Ti lunar samples in which Ti content is largely contributed by ilmenite (Gillis et al., 2006). However, the TiO₂ concentration estimated using this method for lunar surfaces with low-Ti contents is inconsistent with the chemical data of returned samples.

Although spectral contrast (Johnson et al., 1977, 1991a, 1991b) and spatial resolution (Melendrez et al., 1994) have been improved to modify the TiO₂ mapping method used by Charette et al. (1974), the derived TiO₂ concentration using this improved correlation still has large uncertainties especially for the low-Ti materials (Pieters et al., 1993). Methods have been developed to estimate the TiO₂ concentration for lunar soils using new spectral algorithms (Blewett et al., 1997; Lucey et al., 1998, 2000; Gillis et al., 2003, 2006); however, each of these methods appear to have systematic errors (Gillis et al., 2003; Elphic et al., 2002).

Higher spatial resolution, well designed UV–VIS channels, and better coverage by the Wide Angle Camera (WAC) on the Lunar Reconnaissance Orbiter (LRO) (Robinson et al., 2010, 2011) makes the spectral features of various sampled geological units more specific and clear, and thus improving the correlation between orbital UV–VIS data and ground-truth samples (e.g., Jolliff et al., 2009;

* Corresponding author at: MLR Key Laboratory of Saline Lake Resources and Environments, Institute of Mineral Resources, CAGS, Beijing 100037, China.

E-mail address: weigang.kong@gmail.com (W.G. Kong).

Robinson et al., 2011, 2013); however, there remains a lack of understanding of the fundamental mechanisms underlying the UV–VIS–TiO₂ relation.

Two explanations have been proposed for the UV–VIS–TiO₂ relation. In the first one, ilmenite abundance dominates the spectral slope (Wells and Hapke, 1977; Rava and Hapke, 1987), and a precise UV–VIS–TiO₂ relation relies on an accurate UV–VIS–ilmenite relation. In the second one (Pieters, 1978; Pieters et al., 1993), charge transfer between Fe and Ti imparts a very low reflectivity to the Ti-rich components (Bell et al., 1976; Burns et al., 1976). This effect makes the reflectance of high-Ti soils surface dominated, so the spectral variations of components other than Ti are masked. However, in the low-Ti soils, light can pass through more grains, and components other than Fe–Ti oxides exert more influence on the reflectance spectra. The first explanation was supported in a study evaluating the UV–VIS–TiO₂ relation using a combination of Clementine, Lunar Prospector and sample data (Gillis et al., 2006). Results of that study indicated that factors such as ilmenite grain size, modal abundance of plagioclase, and the olivine to pyroxene ratio in mare soils can also influence the UV–VIS spectral slope.

The optical properties of lunar surface materials are also affected by the degree of space weathering (maturity). Materials with longer exposure time to the space weathering environment exhibit a redder slope and reduction of contrast in spectra that mainly results from accumulation of nanophase iron (Fischer and Pieters, 1994). The possible influence of maturity on the UV–VIS slope was discussed by Gillis et al. (2006). Therefore, laboratory investigations for the influence of these factors on the UV–VIS slope are needed to obtain an accurate UV–VIS–TiO₂ relation. Results of such investigations may lead to additional improvements in global mapping of the TiO₂ composition of the lunar surface.

To study the influence of sample factors on the UV–VIS slope, we first obtain the modal abundances, ilmenite grain sizes and shapes, Ti distribution among host mineral, lithic, and glass components in size fractions of selected lunar soils, and in the future, we will investigate their influence on the UV–VIS slope by comparing with their spectra. Much work previously done by the Lunar Soil Characterization Consortium (Taylor et al., 1996, 2001) showed trends in bulk composition in which Ti concentration decreases in successively finer grain size fractions and showed variations in modal mineralogy determined by electron microprobe point counting. Our approach differs in that we are focusing on variations specifically in the hosts of Ti in specific sieve size fractions.

We have done laboratory analyses of lunar soil samples using a combined digital imaging (backscattered electron image and X-ray maps) method to obtain quantitative results. In this study, we report on the Ti distribution in two Ti-rich soils, 10084 from Apollo 11 and 71501 from Apollo 17. This work is a continuation and a combination of previous work reported by Johnson et al. (2009). The questions we address include:

- (1) How is Ti distributed quantitatively among its mineral and lithologic hosts, including volcanic and impact glasses and agglutinates?
- (2) How does the Ti distribution vary among grain size fractions?
- (3) How does the Ti distribution vary with maturity?

2. Digital imaging method

Optical microscopic techniques combined with point counting were first used to investigate the lithic and glass fragment proportions of lunar soils (e.g., Heiken and McKay, 1974; Labotka et al., 1980). Using point counting, precise area proportions of fragments

can be obtained from microscopic images of a “cross section” of the studied sample, and the obtained area proportions of fragments are assumed to approximately equal their volume proportion with a representative image area counted. The abundances of fragments from the optical microscopy technique are referred to as soil “modal” abundances (e.g., Papike et al., 1982), and these results formed the basis for soil genesis studies. However, with optical microscopy it is difficult to obtain true modal abundances owing to mineral and glass components locked in multiphase lithic fragments (Higgins et al., 1996; Taylor et al., 1996, 2001), some of which contribute significantly to the total abundances as demonstrated by Chambers et al. (1994, 1995). On the other hand, electron-beam digital-imaging methods have been used effectively to obtain mineral and glass modal abundances by a combined analysis of both the characteristic X-ray images and back-scattered-electron (BSE) images of lunar soils (e.g., Higgins et al., 1994, 1995, 1996; Chambers et al., 1994; Taylor et al., 1996, 2001). Therefore, we use BSE/X-ray maps to quantify Ti abundance and distribution among mineral phases.

3. Samples and data acquisition

Two high-Ti mare basalts from the Apollo 11 and Apollo 17 sample suites were chosen for this study. Lunar regolith sample 10084 is the <1 mm size fraction of the larger 10002 sample of surface material collected near the Apollo 11 lunar module in Mare Tranquillitatis. The bulk TiO₂ concentration of this mature soil (I_S/FeO , <250 μm = 78, Morris, 1978; Morris et al., 1983) is 7.3 wt.% (Laul and Papike, 1980). Sample 71501 is the <1 mm size fraction of the larger 71500 sample of surface material collected at station 1 during the first Apollo 17 traverse, and the bulk TiO₂ concentration of this submature soil (I_S/FeO , <250 μm = 35, Morris, 1978; Morris et al., 1983) is 9.5 wt.% (Apollo 17 P. E. T., 1973). Petrographic studies (Heiken and McKay, 1974; Simon et al., 1981) revealed that the two soils mainly contain pyroxene, plagioclase, ilmenite, basalt lithic fragments, breccias, glasses, and agglutinates.

These two soils have relatively high TiO₂ concentrations compared with all Apollo soils and have different maturities, which reflect different histories of space weathering and breakdown of mineral and lithic grains. Quantifying the grain size, shape, and distribution of ilmenite, and determining Ti distributions in components other than ilmenite, is important for examining the different influence of these factors on the lunar soil spectra.

Each of the two samples was sieved into five different size fractions: >210 μm , 210–100 μm , 100–48 μm , 48–20 μm , and <20 μm . Analyses for size fraction 210–100 μm of 10084 and 71501 were determined by Johnson et al. (2009). We include analysis results of size fractions 100–48 μm and 48–20 μm of both samples, and compare them with that of the size fraction 210–100 μm .

Three size fractions for each of the two selected soils were mounted in epoxy grain mounts, polished, and the polished sections were examined by taking high resolution photos using an optical microscope-camera system to document exposure of grains prior to electron microprobe measurements. The mounted grain samples were then analyzed using the JEOL 8200 electron microprobe at the Department of Earth and Planetary Sciences at Washington University in St Louis. This electron microprobe has five wavelength dispersive spectrometers and a silicon-drift energy-dispersive spectrometer. These spectrometers allowed us to obtain BSE maps and 12-element X-ray maps (all with 1024 \times 1024 pixels) on selected areas of the sample mounts with about 1000 soil grains included.

The spectrometers were calibrated with standards, as follows: Na on albite, Mg on forsterite, Al on anorthite, Si on albite, Mn on Mn-olivine, Fe on synthetic fayalite and hematite, S on pyrite,

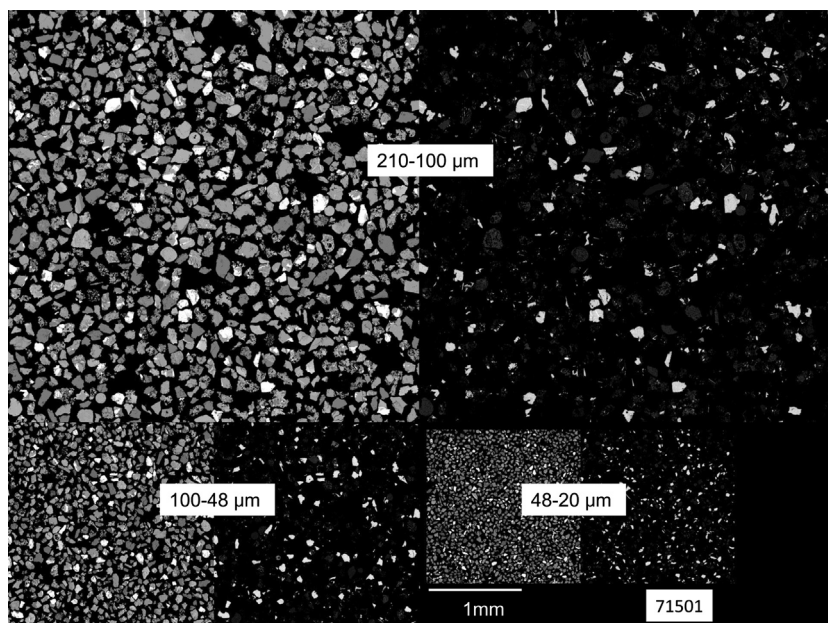


Fig. 1. BSE images (left) and Ti X-ray images (right) of the three grain size fractions of lunar soil sample 71501. In the X-ray images, brightness reflects the Ti concentration. The bright grains are mostly ilmenite and gray grains are mostly Ti-bearing glasses. The Ti X-ray images have been stretched to optimize ilmenite brightness and to enhance mid-level Ti concentrations.

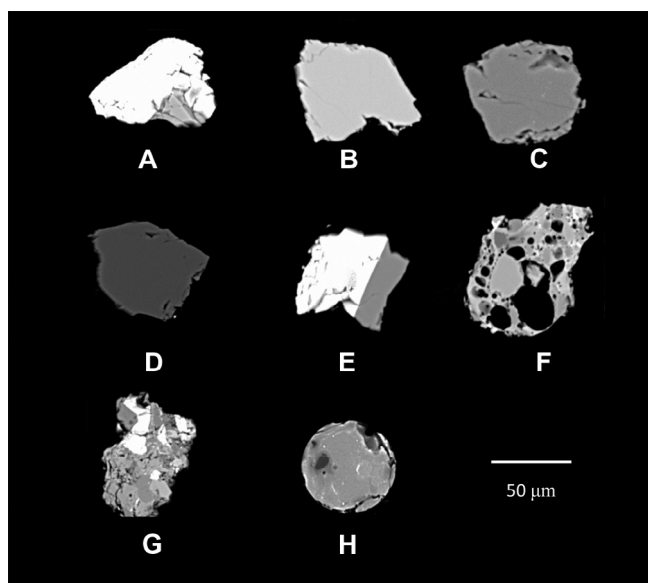


Fig. 2. High resolution BSE images of eight typical petrographic components classified for this study. (A) Ilmenite, (B) olivine, (C) pyroxene, (D) plagioclase, (E) basalt, (F) agglutinate, (G) breccia, and (H) glass.

Ni on NiO, K on microcline, Ca on wollastonite, Ti on rutile, and Cr on Cr_2O_3 . All data were collected at 15 keV accelerating voltage and 25 nA beam current. After obtaining BSE maps and X-ray maps, another set of higher-resolution BSE images were collected on the same X-ray map areas to help classify the soil grains. Fig. 1 shows the lower resolution BSE maps and related Ti X-ray maps of three grain-size fractions from 71501.

3.1. Data analysis

We used ImageJ software (provided by the Research Service Branch (RSB) of the National Institute of Health (NIH)) to extract

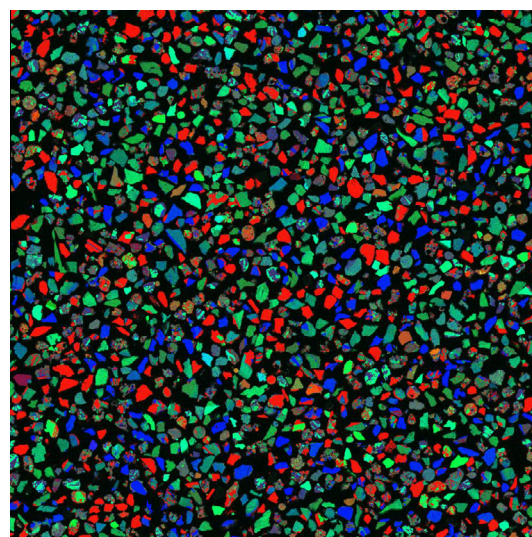


Fig. 3. False color map of soil 71501, 48–20 μm grain size fraction, made from X-ray maps: Al is in the red channel, Mg is in the green channel, and Fe is in the blue channel. In this color scheme, mineralogy appears approximately as follows: red is plagioclase, brightest blue is ilmenite, intermediate to lighter blue or blue–green is ferropoxene and some glass, and green is olivine, magnesian pyroxene, and some glass. (For interpretation of the references to color in this figure legend, the reader is referred to the web version of this article.)

grain size and shape parameters for individual grains using BSE maps and element X-ray maps. Grains in these maps were assigned to one of eight classes (Fig. 2) on the basis of image data, i.e., (A) ilmenite, (B) olivine, (C) pyroxene, (D) plagioclase, (E) basalt, (F) agglutinate, (G) breccia, and (H) glass. We used this classification scheme because (1) multiphase grains are clearly distinguished in the high-resolution BSE images (e.g., Fig. 2), and (2) single phase minerals and glasses show distinct differences in both the BSE images (Fig. 2) and the element X-ray maps (Fig. 3).

To evaluate the characteristic X-ray value or the BSE value of one grain in a specific map, we define $R(x)$ = mean DN value of one grain

Table 1

Defining criteria for grain classification on basis of BSE maps and element X-ray maps. The percentage refers to the area percentage. $R(x)$ refers to the mean DN value of a specific grain in map x over the highest value of that among all the grains in map x .

Classes	Defining criteria
Ilmenite	$R(\text{Ti}) > 0.8$; $R(\text{Si}) < 0.1$; $R(\text{BSE}) > 0.77$
Plagioclase	$R(\text{Al}) > 0.76$; $R(\text{Ca}) > 0.625$; $R(\text{Mg}) < 0.13$; $0.3 < R(\text{BSE}) < 0.44$
Pyroxene	$R(\text{Si}) > 0.37$; $R(\text{Ca}) > 0.1$; $R(\text{Al}) < 0.2$; $R(\text{Ti}) < 0.07$; $0.44 < R(\text{BSE}) < 0.7$
Olivine	$R(\text{Ca}) < 0.27$; $R(\text{Si}) > 0.31$; $0.37 < R(\text{BSE}) < 0.68$
Basalt	<5 vol.% glasses; with two or more minerals
Agglutinates	Void area >5%; "typically with round vesicles"
Breccia	>5 vol.% fine-grain matrix; void area <5%
Glass	Single-phase grains with no match to a mineral composition

in map x /the highest mean DN value of grains in map x . In this definition, the highest mean DN value of grains in map x can approximately represent the mean DN value of a typical mineral with the highest concentration of element x (e.g., an ilmenite grain should have the highest mean $R(\text{Ti})$ value in the Ti X-ray map (excluding any rutile or armalcolite that might be present) for the elemental maps or highest concentration of heavy elements for the BSE map. In reality, the grain with the highest mean DN value was selected carefully to prevent selection of accessory mineral phases with higher concentrations (e.g., rutile in the case of Ti). By this definition, the $R(x)$ value can represent the concentration level of element x of one grain relative to a selected mineral and this value was used as an additional parameter to classify grains. The detailed classification criteria are listed in Table 1. By this classification, we track lithologic components such as basalt and breccia as well as crystalline mineral and glass components because we are interested in how these particles break down into smaller grain sizes as regolith is comminuted during continued meteorite bombardment. On the basis of the $R(x)$ parameters, the false color X-ray images (Fig. 3), and the high resolution BSE images, each grain was individually examined and classified. The area and shape of each grain were determined using ImageJ software. The shape of these grains is defined by the aspect ratio (AR, major axis/minor axis) as follows: AR of 1:1, equant; AR of 2:1 to 1:1, blocky; 5:1 to 2:1, tabular; and >5:1, acicular. About one thousand grains of each grain size fraction of each soil sample were analyzed in this way.

4. Results

4.1. Modal analysis

In the mature soil 10084, agglutinates (38–40 vol.%) dominate in the two coarser size fractions (210–100 μm , 100–48 μm),

Table 2

Modal percentages of mineral and lithic components for the three size fractions of lunar soils 10084 and 71501.

Component	10084					71501				
	210–100 μm	100–48 μm	48–20 μm	150–90 μm^a	45–20 μm^b	210–100 μm	100–48 μm	48–20 μm	150–90 μm^a	45–20 μm^b
Ilmenite	2.40	1.14	2.82	0.90	6.40	4.83	4.94	5.99	5.60	12.3
Plagioclase	7.37	6.88	8.50	5.20	16.8	9.84	10.2	11.5	6.90	16.5
Pyroxene	9.19	8.88	9.97	13.1	16.0	18.1	14.4	21.0	16.6	21.3
Olivine	0.21	0.98	1.00	0.70	1.40	1.70	2.54	4.02	0.50	3.60
Basalt	18.8	30.9	41.3	18.6	53.9	29.0	40.3	39.4	26.3	38.3
Agglutinates	39.7	38.4	28.4	45.9		25.4	20.7	12.0	32.1	
Breccias	17.0	10.9	5.42	5.90		9.00	2.90	2.12	7.10	
Glass	5.29	1.77	1.58	6.40	3.40	2.00	1.95	2.01	4.20	6.70
SiO ₂			0.21				0.42	0.84		
Total vol.%	99.9	99.7	99.0	96.7	97.9	99.8	98.0	98.0	99.3	98.7

^a Data from Taylor et al. (1996).

^b Data from Taylor et al. (2001).

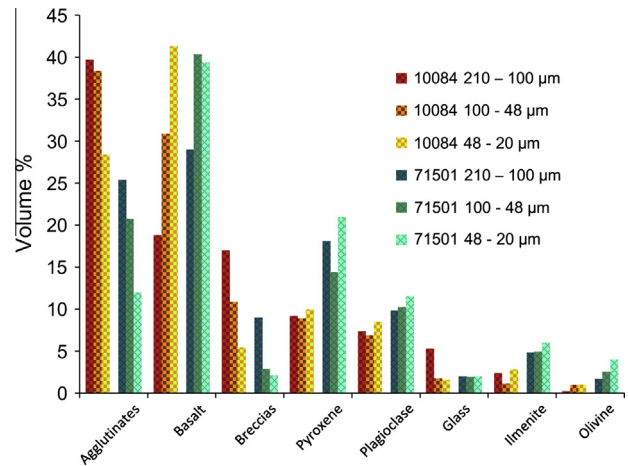


Fig. 4. Results of mineral and lithologic modal analysis for three grain-size fractions of lunar soils 10084 and 71501.

whereas basalts (41.3 vol.%) become dominant in the finer 48–20 μm fraction (Table 2). For all three size fractions, single mineral grains (i.e., ilmenite, pyroxene, olivine, and plagioclase) together comprise 17–23 vol.%, and ilmenite grains only comprise 1–3 vol.% (Table 2).

As grain size decreases among the three fractions of 10084 (Fig. 4), the content of agglutinates decreases from 39.7 to 28.4 vol.% and that of breccias decreases from 17.0 to 5.4 vol.%; whereas the content of basalt increases from 18.8 to 41.3 vol.% and that of ilmenite also has a subtle increase from 1.1 to 2.8 vol.%. In the submature soil 71501, basalts (29.0–38.4 vol.%) and agglutinates (12.0–25.4 vol.%) are generally the two most abundant components; pyroxene (14–21 vol.%) dominates among the single mineral grains (30–43 vol.%), and ilmenite grains comprise about 5–6 vol.% (Table 2).

Among the three size fractions of 71501 (Fig. 4), as grain size decreases, agglutinates content decreases from 25.4% to 12.0 vol.% and breccia content also decreases from 9.0 to 2.1 vol.%; whereas the volume percentages for single mineral grains generally increases (ilmenite, from 4.8 to 6.0; pyroxene, from 14.4 to 21.0; olivine, from 1.7 to 4.0; and plagioclase, from 9.8 to 11.5).

Similarities can be found for both soils (10084 and 71501) (Table 2 and Fig. 4): (1) the most abundant components are agglutinates and basalt fragments, which together account for 50–70 vol.%; and (2) with decreasing grain size, the content of agglutinates and breccias decreases, whereas that of basalts and single mineral grains generally increases. However, many

differences exist between mature soil 10084 and submature soil 71501: (1) the contents of agglutinates (28.4–39.7 vol.%) and breccias (5.4–17.0 vol.%) in mature soil 10084 are higher than those in submature soil 71501 (agglutinates, 12–25 vol.%; breccias, 2–9 vol.%), and (2) the total content of single mineral grains in 10084 (17–23 vol.%) is lower than that in 71501, and the ilmenite grain abundance in 10084 (1–3 vol.%) is less than half of that in 71501 (5–6 vol.%).

4.2. Ilmenite grain shape analysis

In both soils, the shape (by volume) of ilmenite grains is dominated by equant and blocky forms (Table 4). In the mature lunar soil 10084, the shape of ilmenite grains shows a subtle trend of increased AR values (decrease of equant shape with increase of blocky and tabular shapes) as grain size decreases. However, in the submature 71501, no clear trend was found.

5. Discussion

The modal abundance results of this study (Table 2) compare well with the results of previous studies (Heiken and McKay, 1974; Taylor et al., 1996, 2001). The content of single mineral grains determined by Taylor et al. (1996, 2001) also has a trend to increase as grain size becomes finer from the 150–90 μm fraction to the 45–20 μm fraction, which is similar to our results. However, this trend reverses, with single mineral proportion decreasing, among the three size fractions below 45 μm for both soils (Taylor et al., 2001).

5.1. Mass-balance calculation

A forward mass-balance model coupled with the results of our modal analysis was used to investigate the Ti distribution among mineral and lithologic components.

The general mass-balance equation:

$$C_{i,bulk} = \sum_{j=1}^n C_{ij}f_j$$

Table 3

Mass balance calculation for TiO₂ in the size fraction 48–20 μm of lunar soil 71501. The “Mass, not normalized” indicates the relative mass, and the “Average TiO₂ component wt.%” is the average TiO₂ concentration in one specific mineral or lithic components measured using the electron microprobe.

Component	Vol.%	Assumed density g/cm ⁻³	Mass, not normalized	Mass, wt.% normalized	Average TiO ₂ component wt.%	TiO ₂ wt.% contributed	% of Total TiO ₂
Agglutinates	12.0	1.75	21.0	6.79	6.00	0.41	3.80
Basalt	39.4	3.25	127.9	41.3	11.9	4.92	45.8
Glass	2.01	3.00	6.04	1.95	8.50	0.17	1.50
Ilmenite	5.99	4.70	28.1	9.09	52.0	4.73	44.1
Pyroxene	21.0	3.50	73.4	23.7	2.00	0.47	4.40
Olivine	4.02	3.60	14.5	4.67	0.10	0.00	0.00
Plagioclase	11.5	2.70	31.1	10.1	0.00	0.00	0.00
Breccias	2.12	3.00	6.37	2.06	1.50	0.03	0.30
SiO ₂	0.42	2.60	1.09	0.35	0.00	0.00	0.00
Sum	98.4		309.6	100		10.7	

Table 4

Ilmenite grain shape analysis of soils 10084, 71501. The grain shape was classified on the basis of aspect ratio (AR, major axis/minor axis) as follows: AR of 1:1, equant; 2:1 to 1:1, blocky; 5:1 to 2:1, tabular; and >5:1, acicular.

Shape	10084			71501		
	210–100 μm (%)	100–48 μm (%)	48–20 μm (%)	210–100 μm (%)	100–48 μm (%)	48–20 μm (%)
Equant	45.9	39.2	35.0	38	44.8	34.7
Blocky	35.6	38.4	44.2	25.4	20.8	29.4
Tabular	17.4	19.5	19.7	33.9	33.0	34.5
Acicular	1.08	2.85	1.09	2.64	1.42	1.40

was used for this modeling. The variables in the equation are defined as: $C_{i,bulk}$ = mass concentration of element i in bulk sample, $C_{i,j}$ = mass concentration of element i in component j , f_j = mass fraction of component j , and n = number of components. The vol.% determined in this study was used to calculate the mass fraction for each component of the mass-balance equation. In order to calculate mass fraction, the total mass of each component was first calculated by taking the vol.% multiplied by the density of each component (density of each component was adopted from Johnson et al. (2009)). The mass fraction is calculated using the mass of the particular component divided by the total mass of all components. For this study, only the mass concentration of Ti was calculated, and the TiO₂ concentration (wt.%) in each component (j), as determined by EMPA, was multiplied by the corresponding mass fraction of component (j) to obtain the fraction of Ti contained within that particular component. Finally, the fraction of Ti for each component was divided by the total Ti content in all components to obtain the % Ti contributed by each component to the total (bulk) Ti.

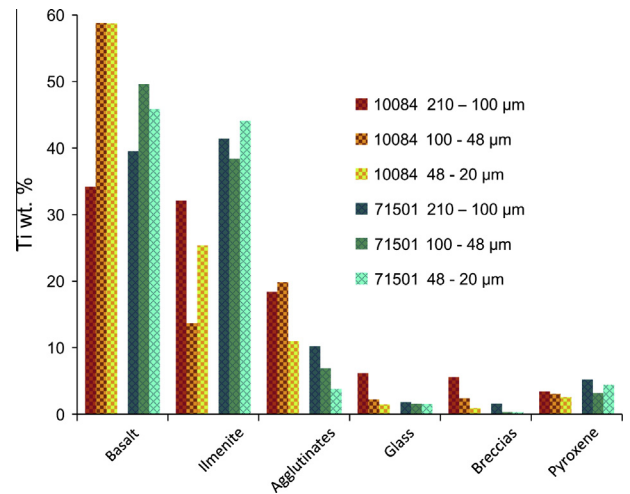


Fig. 5. Ti distribution among six mineral and lithologic hosts in three grain-size fractions of lunar soils 10084 and 71501.

Table 3 lists an example of the mass balance calculation for size fraction 48–20 μm for lunar soil 71501, and the bulk TiO_2 concentration (10.73 wt.%) determined by this study is in good agreement with that of the size fraction 45–20 μm (10.7 wt.%) of lunar soil 71501 as determined by Taylor et al. (2001).

Although it might seem intuitive to equate the Ti content of lunar soils with ilmenite abundance, such a relationship is not strictly the case. Results (Fig. 5) show that most of the Ti in 10084 and 71501 is hosted in free ilmenite or basalt grains. In basalt grains, most, but not all, of the Ti is also in ilmenite, but this ilmenite is of finer grain size. In 71501, about 80–90 wt.% of the Ti is in free ilmenite and basalt grains, with Ti distributed almost equally in free ilmenite grains (38.4–44.1 wt.%) and in finer ilmenite grains bounded in basalts (39.5–49.6 wt.%). In 10084, basalt and ilmenite host about 65–85 wt.% of the Ti, with basalt grains (34.2–58.8 wt.%) hosting more Ti than free ilmenite grains (13.7–32.1 wt.%). In 10084, 10–20 wt.% of Ti occurs in agglutinates, whereas in 71501, a less mature soil, ~4–10 wt.% of Ti occurs in agglutinates. The content of Ti in glasses, breccias, and pyroxene sum up to ~10 wt.% or less in both soils.

6. Summary and future work

The dominant Fe–Ti oxide mineral in lunar soils 10084 and 71501 (grain size fraction 210–20 μm) is ilmenite; other Ti-rich oxides (armalcolite, ulvöspinel, and rutile) are very rare. In both soils, the volume percent of agglutinates and breccias decreases as grain size decreases, and the volume percentages of single mineral grains have a consistent trend to increase as grain size decreases. This trend might have resulted from the breakdown of multiphase lithic fragments into finer, single mineral grains.

In mature soil 10084, more Ti is hosted in basalt as fine-grained ilmenite compared to the coarse, free ilmenite grains. In submature soil 71501, Ti is hosted almost equally by coarse-grained ilmenite and finer-grained ilmenite bound in basalts. This difference likely reflects initial basalt (ilmenite) characteristics. No unique trend was found on the Ti-content distribution variation among these grain-size fractions, whereas the ilmenite shape in mature soil 10084 shows a subtle trend.

Future work will include the analysis of <20 μm grain fraction to compare with these results and those of Taylor et al. (2001). We will analyze additional lunar soils that cover a range of Ti concentrations (Apollo 12, Apollo 15) and levels of maturity. Subsequently, coupling our results and those of Taylor et al. (2001), we will compare results from the quantitative sample petrography to the UV–VIS spectra of the grain-size fractions to determine correlations between the Ti distribution and the UV–VIS ratio.

Acknowledgments

We thank Randy Korotev and Ryan Zeigler for providing their expertise and instructions to Weigang Kong. We also thank the Basic Research and Operating Fund (K0903) for supporting Weigang Kong's work at CAGS during the draft of manuscript and the scholarship from Chinese Educational council for supporting Weigang Kong's study at Washington University in St. Louis as a joint-training PhD student from Shandong University. We gratefully acknowledge Washington University and the McDonnell Center for space sciences for their support to the planetary material research group in the Dept. of Earth and Planetary Sciences, Washington University. We thank prof. Oded Aharonson and two anonymous reviewers for their help on handling and improving the manuscript.

References

- Bell, P.M., Mao, H.K., Weeks, R.A., 1976. Optical spectra and electron paramagnetic resonance of lunar and synthetic glasses: A study of the effects of controlled atmosphere, composition, and temperature. *Proc. Lunar Sci. Conf.* 7, 2543–2559.
- Blewett, D.T., Lucey, P.G., Hawke, B.R., Jolliff, B.L., 1997. Clementine images of the lunar sample-return stations: Refinement of FeO and TiO_2 mapping techniques. *J. Geophys. Res.* 102, 16319–16325.
- Burns, R.G., Parkin, K.M., Loeffler, B.M., Leung, I.S., Abu-Eid, R.M., 1976. Further characterization of spectral features attributable to titanium on the Moon. *Proc. Lunar Sci. Conf.* 7, 2651–2578.
- Chambers, J.G., Patchen, A., Taylor, L.A., Higgins, S.J., McKay, D.S., 1994. Lunar mineral feedstocks from rocks and soil: X-ray digital-imaging in resource evaluation. *Lunar. Planet. Sci.* XXV, 235–236.
- Chambers, J.G., Taylor, L.A., Patchen, A., McKay, D.S., 1995. Quantitative mineralogical characterization of lunar high-Ti mare basalts and soils for oxygen production. *J. Geophys. Res. – Planets* 100, 14391–14401.
- Charette, M.P., McCord, T.B., Pieters, C.M., Adams, J.B., 1974. Application of remote spectral reflectance measurements to lunar geology classification and determination of titanium content of lunar soils. *J. Geophys. Res.* 79 (11), 1605–1613.
- Elphic, R.C. et al., 2002. The lunar prospector neutron spectrometer constraints on TiO_2 . *J. Geophys. Res.* 107 (E4), <http://dx.doi.org/10.1029/2000JE001460>.
- Fischer, E.M., Pieters, C.M., 1994. Remote determination of exposure degree and iron concentration of lunar soils using VIS–NIR spectroscopic methods. *Icarus* 111, 475–488.
- Gillis, J.J., Jolliff, B.L., Elphic, R.C., 2003. A revised algorithm for calculation TiO_2 concentrations from Clementine UV–VIS data: A synthesis of rock, soil, and remotely sensed TiO_2 concentrations. *J. Geophys. Res.* 108 (E2), 5009. <http://dx.doi.org/10.1029/2001JE001515>.
- Gillis, J.J., Lucey, P.G., Hawke, B.R., 2006. Testing the relation between UV–VIS color and TiO_2 content of the lunar maria. *Geochim. Cosmochim. Acta* 70, 6079–6102.
- Heiken, G., McKay, D.S., 1974. Petrography of Apollo 17 soils. *Proc. Lunar. Sci. Conf.* 5, 843–860.
- Higgins, S.J., Patchen, A., Chambers, J.G., Taylor, L.A., McKay, D.S., 1994. Petrographic characterization of lunar soils: Application of X-ray digital-imaging to quantitative and automated analysis. *Lunar. Planet. Sci.* XXV, 547–548.
- Higgins, S.J., Taylor, L.A., Chambers, J.G., Patchen, A., McKay, D.S., 1995. X-ray digital-imaging analysis: Requisite data for spectral reflectance studies. *Lunar. Planet. Sci.* XXVI, 601–602.
- Higgins, S.J., Taylor, L.A., Chambers, J.G., Patchen, A., McKay, D.S., 1996. X-ray digital imaging petrography: Technique development for lunar mare soils. *Meteorit. Planet. Sci.* 31, 356–361.
- Johnson, T.V., Saunders, R.S., Matson, D.L., Mosher, J.A., 1977. A TiO_2 abundance map for the northern maria. *Proc. Lunar. Sci. Conf.* 8, 1029–1036.
- Johnson, J.R., Larson, S.M., Singer, R.B., 1991a. Remote sensing of potential lunar resources, 1. Near-side compositional properties. *J. Geophys. Res.* 96 (E3), 18861–18882.
- Johnson, J.R., Larson, S.M., Singer, R.B., 1991b. A reevaluation of spectral ratios for lunar mare TiO_2 mapping. *Geophys. Res. Lett.* 18 (11), 2153–2156.
- Johnson, D., Jolliff, B., Zeigler, R., Carpenter, P., 2009. Distribution of Ti in glass and mineral components of lunar soils 10084 and 71501; grain size fraction 100 to 210 μm . *Lunar. Planet. Sci.* 40. Abstract #2346.
- Jolliff, B.L., 1999. Clementine UV–VIS multispectral data and the Apollo 17 landing site: What can we tell and how well? *J. Geophys. Res.* 104 (E6), 14123–14148.
- Jolliff, B.L., Wiseman, S.M., Robinson, M.S., Lawrence, S., Denevi, B.W., Bell, J.F., 2009. LRO Camera Imaging of the Moon: Apollo 17 and other Sites for Ground Truth. *American Geophysical Union* (Fall). Abstract #U31A-0012.
- Labotka, T., Kempa, M., White, C., Papike, J., Laul, J., 1980. The Lunar regolith: Comparative petrology of the Apollo sites. *Proc. Lunar Sci. Conf.* 11, 1285–1305.
- Laul, J.C., Papike, J.J., 1980. The lunar regolith – Comparative chemistry of the Apollo sites. *Proc. Lunar Sci. Conf.* 11, 1307–1340.
- Lucey, P.G., Blewett, D.T., Hawke, B.R., 1998. Mapping the FeO and TiO_2 content of the lunar surface with multispectral imagery. *J. Geophys. Res.* 103 (E2), 3679–3699.
- Lucey, P.G., Blewett, D.T., Jolliff, B.L., 2000. Lunar iron and titanium abundance algorithms based on final processing Clementine UV–VIS images. *J. Geophys. Res.* 105 (E8), 20297–20305.
- Lunar Sample Primary Examine Team, 1973. Apollo 17 lunar samples: Chemical and petrographic description. *Science* 182, 659–672.
- Melendrez, D.E., Johnson, J.R., Larson, S.M., Singer, R.B., 1994. Remote sensing of potential lunar resources, 2. High spatial resolution mapping of spectral reflectance ratios and implications for near side mare TiO_2 content. *J. Geophys. Res.* 99 (E3), 5601–5619.
- Morris, R.V., 1978. The surface exposure (maturity) of lunar soils: Some concepts and Is/FeO compilation. *Proc. Lunar Planet. Sci. Conf.* 9, 2287–2297.
- Morris, R.V., Score, R., Dardano, S., Heiken, G.H., 1983. *Handbook of Lunar Soils*, Planetary Materials Branch, Publication 67.
- Papike, J.J., Simon, S.B., Laul, J.C., 1982. The lunar regolith – Chemistry, mineralogy, and petrology. *Rev. Geophys.* 20, 761–826.
- Pieters, C.M., 1978. Mare basalt types on the front side of the Moon: A summary of spectral reflectance data. *Proc. Lunar Planet. Sci. Conf.* 9, 2825–2849.

- Pieters, C.M., McCord, T.B., Adams, J.B., 1976. Regional basalt types in the Luna 24 landing area as derived from remote observations. *Geophys. Res. Lett.* 3 (11), 697–700.
- Pieters, C.M., Fischer, E.M., Rode, O., Basu, A., 1993. Optical effects of space weathering: The role of the finest fraction. *J. Geophys. Res.* 98 (E11), 20817–20824.
- Rava, B., Hapke, B., 1987. An analysis of the Mariner 10 color ratio map of Mercury. *Icarus* 71 (3), 397–429.
- Robinson, M.S. et al., 2010. Lunar Reconnaissance Orbiter Camera (LROC) instrument overview. *Space Sci. Rev.* 150, 81–124.
- Robinson, M.S., Denevi, B.W., Sato, H., Hapke, B., Hawke, B.R., 2011. LROC WAC ultraviolet reflectance of the Moon. *Lunar. Planet. Sci.* 42. Abstract #1842.
- Robinson, M.S., Sato, H., Denevi, B.W., Plescia, J.B., Jolliff, B.L., 2013. Color of the Moon: LROC WAC 320 to 689 nm. European Planetary Science Congress, University College London.
- Shkuratov, Y., Kaydash, V., Korokhin, V., Velikodsky, Y., Opanasenko, N., Videen, G., 2011. Optical measurements of the Moon as a tool to study its surface. *Planet. Space Sci.* 59, 1326–1371.
- Simon, S.B., Papike, J.J., Laul, J.C., 1981. The lunar regolith: comparative studies of the Apollo and Luna sites. *Petrology of soils from Apollo 17, Luna 16, 20, and 24. Proc. Lunar Planet. Sci.* 12B, 371–388.
- Taylor, L., Patchen, A., Taylor, D., Chambers, J., McKay, D., 1996. X-ray digital imaging petrography of lunar mare soils: Modal analyses of minerals and glasses. *Icarus* 124, 500–512.
- Taylor, L., Pieters, C., Keller, L., Morris, R., McKay, D., 2001. Lunar mare soils: Space weathering and the major effects of surface-correlated nanophase Fe. *J. Geophys. Res.* 106, 27985–27999.
- Wells, E., Hapke, B., 1977. Lunar soil: Iron and titanium bands in the glass fraction. *Science* 195, 977–979.